How to cite: *Angew. Chem. Int. Ed.* **2023,** *62,* e202215600
International Edition: doi.org/10.1002/anie.202215600
German Edition: doi.org/10.1002/ange.202215600

Zn Metal Batteries

Monolithic Phosphate Interphase for Highly Reversible and Stable Zn Metal Anode

Sailin Liu, Jitraporn (Pimm) Vongsvivut, Yanyan Wang, Ruizhi Zhang, Fuhua Yang, Shilin Zhang, Kenneth Davey, Jianfeng Mao, and Zaiping Guo**

Abstract: Zinc metal battery (ZMB) is promising as the next generation of energy storage system, but challenges relating to dendrites and corrosion of the zinc anode are restricting its practical application. Here, to stabilize Zn anode, we report a controlled electrolytic method for a monolithic solid-electrolyte interphase (SEI) via a high dipole moment solvent dimethyl methylphosphonate (DMMP). The DMMP-based electrolytes can generate a homogeneous and robust phosphate SEI ($Zn_3(PO_4)_2$ and ZnP_2O_6). Benefiting from the protecting impact of this in situ monolithic SEI, the zinc electrode exhibits long-term cycling of 4700 h and a high Coulombic efficiency 99.89 % in Zn|Zn and Zn|Cu cell, respectively. The full V_2O_5|Zn battery with DMMP-H_2O hybrid electrolyte exhibits a high capacity retention of 82.2 % following 4000 cycles under 5 A g^{-1}. The first success in constructing the monolithic phosphate SEI will open a new avenue in electrolyte design for highly reversible and stable Zn metal anodes.

Introduction

Zinc metal batteries (ZMBs) are practically promising for energy storage because of low-cost and potential for large-scale application. However, significant drawbacks include formation of dendrites, corrosion and hydrogen evolution reaction (HER) from the Zn anode.[1] Because Zn nucleation and growth are significantly influenced via the chemical nature of the electrolyte, it is important to develop electrolyte that has good stability with Zn anode and to form a uniform, robust solid electrolyte interphase (SEI) on the metal anode ZMB.[2] It is however practically difficult to design a stable and in situ SEI for Zn in aqueous electrolyte because of water splitting reaction and a lack of passivating components in the electrolyte.[3] Compared with apparently established knowledge of SEI formation with lithium-ion batteries (LIBs), the current understanding of in situ SEI for ZMB is still in its early stage.[4] An ideal SEI is electronically insulating, has high ionic conductivity, exhibits self-passivating behaviour and is stable against dissolution. Therefore, exploring suitable SEI compositions and structure are essential for the further development of ZMB towards long term cycling life.

Amongst components for metal protection, zinc phosphate coating is common because it promotes adhesion and has wear-resistance on steels and alloys.[5] Insoluble phosphate layer has good binding to substrate metal because of chemical bonding between the coating and the matrix,[6] which is attractive as SEI in ZMBs. A few successful attempts to build phosphate containing SEI on Zn anode are reported using electrolyte additives[7] or organic solvents,[8] including, $Zn(H_2PO_4)_2$, tris (2,2,2-trifluoroethyl) phosphate (TFEP),[9] trimethyl and triethyl phosphate (TMP and TEP).[10] These works demonstrated that phosphate SEIs have good Zn^{2+} conductivity, high interface energy and corrosion-inhibition. Importantly, except for obtaining the protective phosphate component, the SEI structure is also important in alleviating the dendrite growth. Currently reported SEIs are composed, normally, of two or more compositions, and represent mosaic or multilayer structure, such as ZnF_2-$Zn_5(CO_3(OH)_6$-$Zn(NO_3)_2)_2$-organic bilayer,[11] combined $Zn_3(PO_4)_2$ and ZnF_2,[12] and poly-ZnP_2O_6[13] and

[*] Dr. S. Liu, Y. Wang, R. Zhang, Dr. F. Yang, Dr. S. Zhang, Prof. K. Davey, Dr. J. Mao, Prof. Z. Guo
School of Chemical Engineering and Advanced Materials, the University of Adelaide
Adelaide SA-5005 (Australia)
E-mail: jianfeng.mao@adelaide.edu.au
zaiping.guo@adelaide.edu.au

Dr. J. (. Vongsvivut
Australian Synchrotron, Australia's Nuclear Science and Technology Organisation
Clayton VIC-3168 (Australia)

R. Zhang, Prof. Z. Guo
Institute for Superconducting and Electronic Materials, Australian Institute for Innovative Materials, the University of Wollongong
Wollongong, NSW-2500 (Australia)

R. Zhang
Department of Chemical and Process Engineering, Faculty of Engineering and Physical Sciences, University of Surrey
Guildford, Surrey, GU2 7XH (UK)

ZnF_2. Although these interphases do improve cycling stability of the Zn anode, pulverization remains problematic especially following long term cycling, possibly because of poor integrity and complex composition of the SEI-layer.

For LIBs it is conjectured that a highly homogeneous, dense and inorganic-rich SEI could obviate pulverization of the Li metal anode.[14] However, this monolithic SEI has not yet been reported for ZMBs, most likely because of the lack of electrolyte components to give robust, uniform inorganic species. It would be a significant boost for practical development of ZMBs therefore if an electrolyte can be devised to build an in situ robust monolithic phosphate protective interphase on the Zn metal anode.

Here, we report for the first time, an organophosphorus fire-retardant solvent DMMP with a high electric dipole moment of 3.62 D for generating an in situ monolithic phosphate SEI on Zn anode. The high dipole moment solvent with a high polarity attracts, or repels, valence electrons from other compounds and generates reactions through electron transfer, which permits a rapid SEI formation.[15] In contrast to solvents that include carbonates, ethers, esters, sulfones and nitriles used in LIBs, DMMP is usually used as a fire-retardant in LIBs and not for producing SEI.[16] We show however that for Zn anode, the high dipole moment of DMMP significantly favours phosphating conversion reaction that can be used to control reductive decompositions and interphase chemistry. Organic and hybrid electrolyte with DMMP solvent exhibited two advantageous features, namely, 1) predominated DMMP reduction that leads to phosphate SEI on the Zn anode, and; 2) a highly monolithic and homogeneous SEI of $Zn_3(PO_4)_2$ and ZnP_2O_6. Compared with reported organic solvents with high dipole moment (>3D), including, acetonitrile (AN),[17] propylene carbonate (PC),[18] dimethyl sulfoxide (DMSO)[19] and N,N-Dimethylformamide (DMF),[20] the interphase derived from DMMP solvent exhibited boosted cycling stability when transferred to the pure aqueous electrolyte. The Zn|Zn symmetric cell with this DMMP electrolyte presents a superior long cycling of over 4700 hours at 1 mA cm^{-2}, and the Zn|Cu asymmetric cell also shows high reversibility of Zn^{2+} plating/stripping with a Coulombic efficiency (CE) of 99.89 % following 4000 cycles. Additionally, phosphate SEI derived in the hybrid DMMP-H_2O evidenced consistency with organic DMMP electrolyte, highlighting the practical potential for use in water-based electrolyte. This hybrid electrolyte exhibits a greater corrosion potential and lower corrosion current than the aqueous electrolyte and inhibits Zn dendrite formation together with HER reaction, leading to 2500 h of cycling in symmetric Zn|Zn batteries. A full V_2O_5|Zn battery with the DMMP-based hybrid electrolyte exhibited a high-capacity retention rate of 82.2 % for 4000 cycles at 5 A g^{-1}.

This work demonstrates that phosphate solvent with high dipole moment can be used to design monolithic SEI to boost long-term cycling stability. The success of this high dipole moment solvent strategy for readily stabilizing the Zn anode could open the way to a flexible in situ SEI design by bringing the desired components close to the electrode surface to facilitate redox reaction and yield a homogeneous phosphate conversion coating layer.

Results and Discussion

Novel Zn(OTf)$_2$-DMMP Non-Flammable Electrolyte

Solvent is important in controlling metal ion coordination environment and electrolyte properties. A solvent with strong solvating ability with Zn^{2+} has greater opportunity to form solvent-derived SEI, and a greater desolvation barrier. Solvents with a high dipole moment (D) generate fast interfacial reactions for SEI formation, however decomposed components may not be suitable for regulating growth of Zn dendrites and inhibiting corrosion. Therefore, the solvent in electrolyte needs good both physical properties and electrochemical performance.

Organic solvents that exhibit high D value reported for ZMBs, such as AN, PC, DMF and DMSO, do not result in phosphate interphase because of the lack of phosphorous element. In comparison, fire-retardant phosphate solvents including, TEP, TMP and DMMP exhibit a high dipole moment >2.5 D, moderate dielectric constant <25, low viscosity <2 mPa s and non-combustibility, Figure 1a (Figures S1–3), together with the ability to generate phosphate SEI. Although TEP and TMP were previously reported to form zinc phosphates containing SEI[10b,21] for preventing Zn anode from corrosion, DMMP is supposed to be a better candidate because of its much higher dipole moment (3.62D), which could possibly facilitate faster phosphating conversion reaction than TEP and TMP solvents.

To confirm the impact of dipole moment on Zn anode stability, the cycling performance for symmetric Zn|Zn and asymmetric Zn|Cu cells were compared. For solvents with greater D value than DMMP, Zn|Zn symmetric cells with 0.5 M-Zn(OTf)$_2$-AN, 0.5 M-Zn(OTf)$_2$-PC, 0.5 M-Zn(OTf)$_2$-DMSO and 0.5 M-Zn(OTf)$_2$-DMF electrolyte (abbreviated, respectively, as AN, PC, DMSO and DMF electrolyte) all exhibited less cycling stability than for 0.5 M-Zn(OTf)$_2$-DMMP (DMMP electrolyte), which exhibited a cycle life over half a year, Figure 1b. For phosphate solvents, 0.5 M-Zn(OTf)$_2$-DMMP electrolyte exhibited excellent reversibility in Zn|Cu batteries as is seen in Figures 1c–e (and Figure S4) with a high mean CE of 99.91 % following 2000 cycles at 0.1 mA cm^{-2} (Figure 1c), and 99.89 % following 4000 cycles at 0.5 mA cm^{-2} (Figure 1d). Amongst the electrolytes with phosphate-based solvent, the nucleation overpotential for Zn in DMMP electrolyte of 0.176 V evidences its significantly low deposition barrier for Zn^{2+}, Figure 1e.

The Zn|Zn battery with DMMP electrolyte exhibited the most stable cycle life of up to 4700 h, together with smallest polarization potential of 160 mV of the three phosphate-based electrolytes under current density 1 mA cm^{-2} (Figure S5). This 'good' performance with DMMP for Zn metal is attributed to its greater D value compared with TEP and TMP, that boosts phosphating conversion at the Zn metal surface and enhances Zn ion reversibility. The protective impact of the interphase gen-

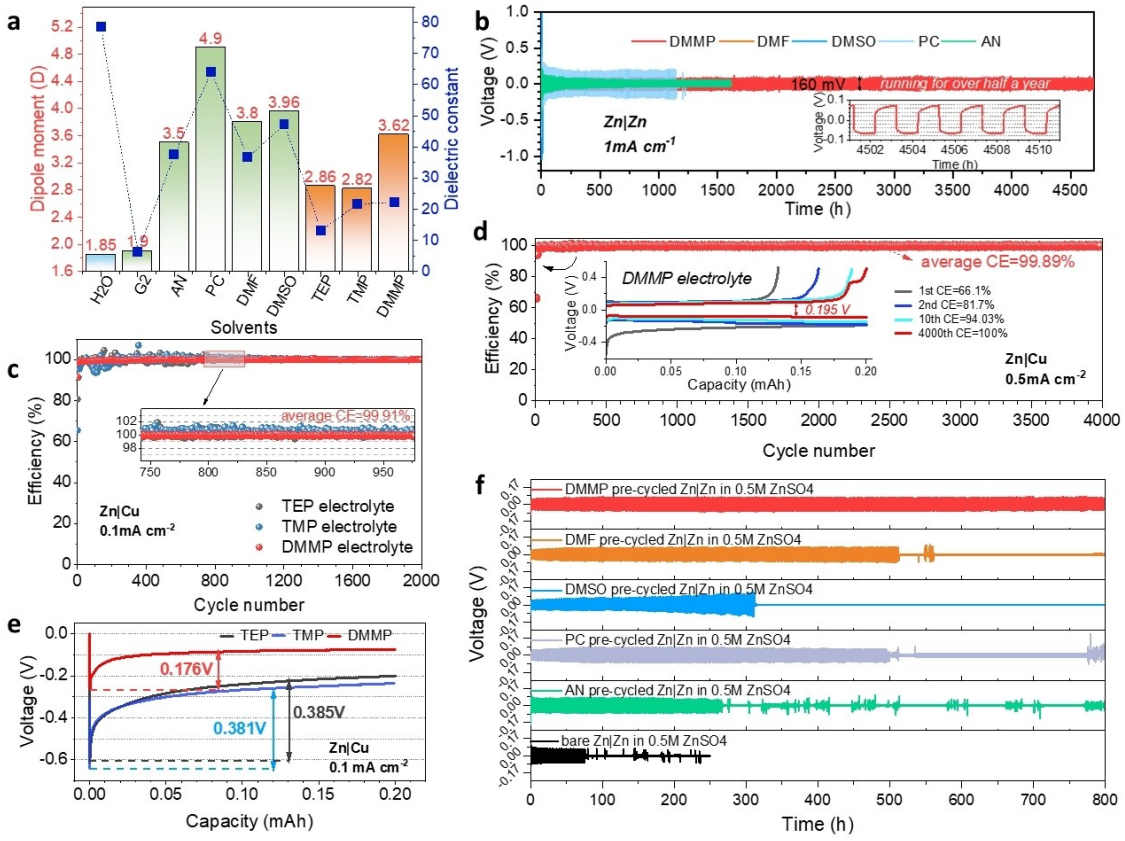

Figure 1. Physical property of organic solvents and electrochemical performance for Zn metal in differing organic electrolytes. (a) Comparison of physical parameters of reported organic solvents with this work in ZMBs. (b) Cycling of Zn | Zn symmetric battery in electrolyte with organic solvent (DMMP, DMF, DMSO, PC and AN) under test current density 1 mA cm^{-2}. (c) CEs for Zn | Cu battery with 0.5 M-Zn(OTf)$_2$-DMMP, 0.5 M-Zn(OTf)$_2$-TMP and 0.5 M-Zn(OTf)$_2$-TEP electrolyte under 0.1 mA cm^{-2}. (d) CE and plating/stripping profiles of Zn | Cu batteries with 0.5 M-Zn(OTf)$_2$-DMMP at the current density of 0.5 mA cm^{-2}. (e) Nucleation overpotential for Zn | Cu asymmetric cells under TEP, TMP and DMMP solvent-based electrolytes. (f) Cycling performance for Zn | Zn symmetric battery in 0.5 M-$ZnSO_4$-H_2O electrolyte with Zn electrodes pre-cycled in organic solvent-based electrolyte.

erated from DMMP electrolyte is also evidenced by performance of the pre-cycled and bare Zn electrodes in 0.5 M-$ZnSO_4$-H_2O electrolytes, as is shown in Figure 1f. Without protection, the bare Zn electrode exhibits a short cycle life of *ca.* 50 cycles, whilst with interphase protection, the pre-cycled electrode exhibits a greater cycling of up to 730 cycles. Additionally, the pre-cycled Zn electrode in DMMP maintains a significantly better cycling stability in aqueous 0.5 M-$ZnSO_4$-H_2O electrolyte than that for pre-cycled electrodes in AN, PC, DMMP and DMF electrolytes, Figure 1f. The boosted cycling performance of the DMMP-derived interphase protected Zn electrode in 0.5 M-$ZnSO_4$-H_2O electrolyte evidences the protection of DMMP solvent derived SEI.

Interfacial Chemistry

To establish the Zn anode passivation mechanism in Zn-(OTF)$_2$-DMMP, interfacial morphology and composition of cycled Zn metal electrodes from different phosphate solvent-based electrolytes and organic electrolytes were determined using judiciously combined, scanning microscopy (SEM), optical microscopy, focused ion beam (FIB) and X-ray photoelectron spectroscopy (XPS).

SEM characterized images (Figure S6) showed that Zn deposition in TEP and TMP was less even than that in DMMP electrolyte. The cycled morphology of Zn electrodes from high dipole moment solvent-based electrolytes, AN, PC, DMSO and DMF, are not as uniform as for DMMP electrolyte (Figure S7). Following 10 cycles, the Zn electrodes cycled with TEP and TMP exhibited some 'dead' Zn dendrites on the separators, as is evidenced in Figure S8. However, DMMP resulted in a smooth stripping/plating interface on the Zn electrode with no zinc dendrites on the separator as is demonstrated in Figure 2a (and Figure S8).

Real-time optical microscopy findings confirmed (Figure S9) that Zn dendrites are not likely to occur in DMMP compared with TEP and TMP electrolyte at significant large current density 10 mA cm^{-2}. These microscopic differences evidence that DMMP favours a more reversible Zn^{2+} ion plating/stripping behaviour than TEP and TMP based

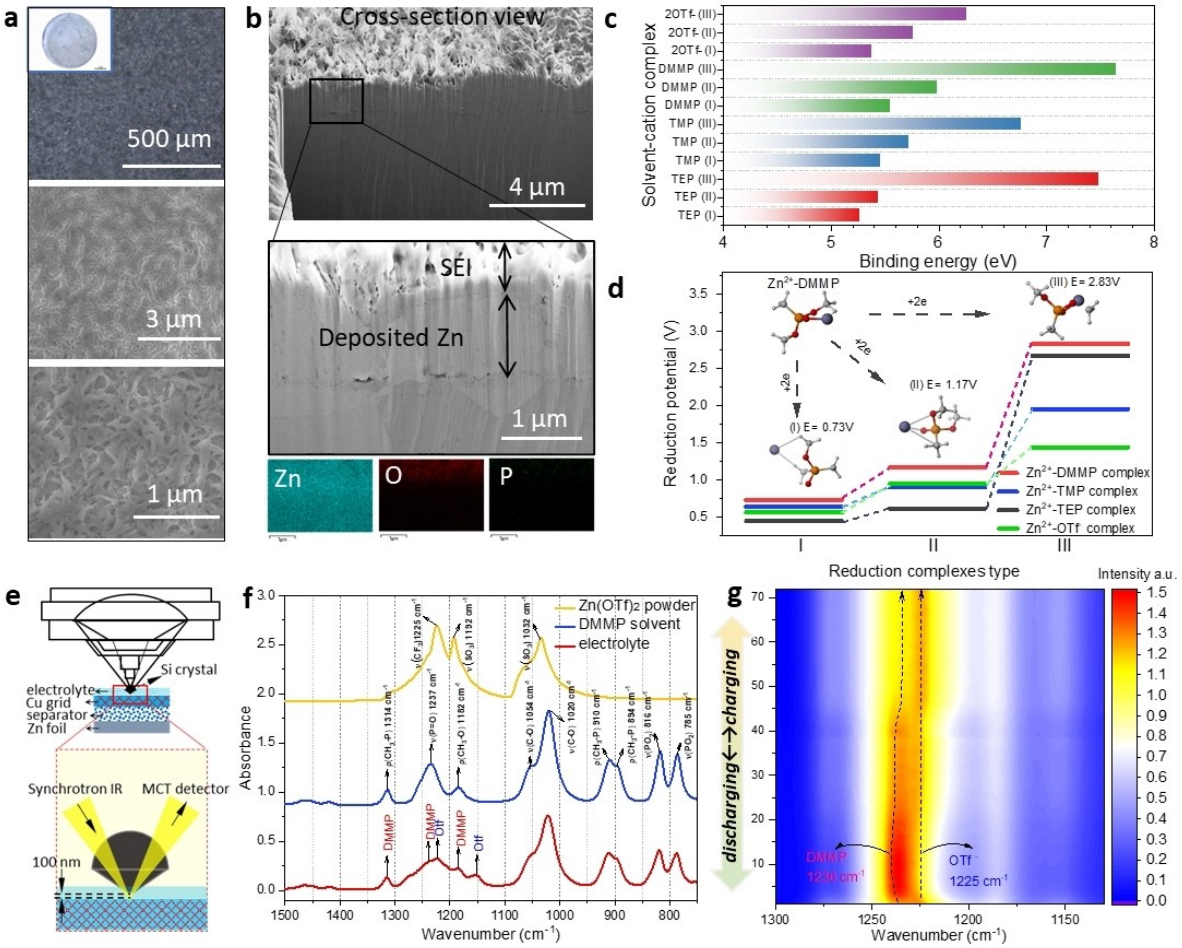

Figure 2. Interfacial characterization and decomposition mechanism for 0.5 M-$Zn(OTf)_2$-DMMP electrolyte on Zn electrode. (a) Optical microscope and SEM image of morphology at the Zn anode following plating/stripping for 10 cycles. (b) Focused Ion Beam Scanning Electron Microscopy (FIB-SEM) image of cross-section of cycled Zn electrode with deposited Zn. (c) Computed binding energy for solvent-cation complexes (I to III represent binding energy of top three stable solvent-Zn^{2+} complexes for each organic solvent). (d) Comparison of reduction potential for TEP, TMP, DMMP solvent and anion complexed with Zn^{2+}. (e) Illustration of piezo-controlled macro-ATR monitoring of interfacial area of electrode. (f) Peak assignments of FT-IR spectra for $Zn(OTf)_2$ powder, DMMP solvent and 0.5 M-$Zn(OTf)_2$-DMMP electrolyte. (g) Contour plot for in situ ATR spectra for Cu electrode during Zn^{2+} plating/stripping in Zn|Cu battery with 0.5 M-$Zn(OTf)_2$-DMMP electrolyte.

electrolytes. In-depth interfacial analyses using FIB and XPS confirmed the advantage of DMMP solvent is because of strong phosphating ability in forming a robust interphase on Zn electrode during cycling. As is evidenced in Figure 2b, the Zn electrode following plating in DMMP electrolyte exhibited a dense Zn deposition of *ca.* 1 µm, underneath an interphase consisting of Zn, P and O. This interphase exhibits a cross-linked morphology when viewed from the top (plan view), which is robust at the bottom under the cross-sectional view (side elevation), as shown in Figure 2a (and Figure S10). XPS results of Figure S11 underscore that DMMP electrolyte results in interphase with greater phosphate content and less fluorine than that for the other two phosphate solvents. This is because of the reduction of salt anions in TEP and TMP electrolyte. The peak-fitting analyses of Figure S12 evidence that the composition of the DMMP electrolyte derived interphase is zinc phosphate, because of no signal for other species.

Theoretical computation and in situ Synchrotron FT-IR findings were used to confirm the formation mechanism of phosphating SEI. Figure 2c presents the top three stable complexes for Zn^{2+} ion with one solvent molecule or anion from model simulation. It is seen from the figure that DMMP-Zn^{2+} species exhibit the greatest binding energy amongst all phosphate solvents and OTf^- anion, showing its strong ability in occupying the inner solvation shell of Zn^{2+} ions.

The reduction potential computation of three different reduction geometries in OTf^- (Figure S13), TEP (Figure S14), TMP (Figure S15) and DMMP (Figure S16 and Figure 2d) was compared. It was found that all three reduction geometries for the DMMP–Zn complex favour

greater reduction potential, evidencing a preferential decomposition for DMMP *vs.* TEP and TMP that is in agreement with reported findings.[22] The in situ Synchrotron FT-IR detected 100 nm depth of electrolyte above the Zn electrode surface and directly evidenced highly significant reduction behaviour of the DMMP molecule at the discharging state, as illustrated in Figure 2e (and Figure S17).

The peaks for electrolyte components were assigned prior to analyses as is shown in Figure 2f. During discharging/charging, the Zn electrode interface was detected with apparent reversible changes in peak intensity as seen in Figure 2g. When the monitored electrode was discharging, the intensity of the peak at 1236 cm^{-1},[23] which corresponds to vibration of P=O bond from DMMP solvent, as is identified in Figure 2f, got stronger, whilst the intensity for the SO_3 vibration for OTf^- anion at 1225 cm^{-1}[24] became weaker. When shifted to the charging state, the intensity of the peaks from the electrolyte components recovered to static status. Importantly, these in situ findings accord with the high D value for DMMP, which supports rapid phosphating SEI formation reaction, and suppression of anion decomposition at the interface.

$Zn(OTf)_2$-DMMP-H_2O Hybrid Electrolyte

It is established that water molecules boost Zn intercalation/deintercalation kinetics in cathode materials including, V_2O_5. Compared with aqueous electrolyte, the organic electrolyte has reduced kinetics under high current density.[25] Therefore, to take advantage of the phosphating interphase derived from DMMP solvent, and to improve the full cell performance of the organic electrolyte, a controlled proportion of water (molar ratio DMMP:H_2O is 3:2 (a volume ratio 9:1) and denoted as DMMP-H_2O electrolyte) was added to the DMMP electrolyte. To confirm whether introduction of water will change the formation of SEI on Zn anode, the aqueous electrolyte, organic electrolyte and organic/aqueous hybrid DMMP-H_2O electrolyte were compared with the symmetric Zn|Zn cell. As shown in Figures 3a–b, (and Figure S18), the Arrhenius equation was used to compute the activation energy for Zn^{2+} ions through fitting of Nyquist plots of Zn symmetric cells at differing temperatures. The activation energy, E_{a1} and E_{a2}, respectively, represents the transport barrier to Zn^{2+} ions in the SEI, and the desolvation barrier for Zn^{2+} in the electrolyte at the Zn surface.[13] For aqueous electrolyte, there is no SEI generated, only by-products on the surface of Zn electrode, and the desolvation energy E_{a2} in 0.5 M-$Zn(OTf)_2$-H_2O electrolyte is 48.49 kJ mol^{-1}. The DMMP based electrolytes all exhibit high transference numbers (Figure S19) and, the derived interphases show good electronically insulating property (Figure S20), which prevents Zn ions from depositing onto the interphase and leads to a zinc deposition underneath the SEI.

In comparison, the activation energies (E_{a1} and E_{a2}) for organic electrolyte and hybrid electrolyte are similar in value, evidencing that the desovaltion value and properties of the phosphating interphases derived from these two electrolytes are very similar. The Near Edge X-ray Absorption Spectroscopy (NEXAFS) for the Zn L-edge following cycling confirmed that SEI compositions generated from DMMP and hybrid DMMP-H_2O electrolyte are the same (Figure S21). Additionally, as is directly compared in Figure 3c, the desolvation energy E_{a2} for organic and hybrid electrolyte are less than for aqueous electrolyte, evidencing that the zinc ions have more difficulty in getting desolvated from water molecules than DMMP based electrolytes. This is because water molecule exhibits a greater dielectric constant of 78 compared with DMMP of 22.3, and means the affinity between water and cation is stronger than between DMMP and cation.

The significant desolvation energy, $E_{a2} = 48.49$ kJ mol^{-1} for Zn ions in the 0.5 M-$Zn(OTf)_2$-H_2O electrolyte results in 'parasitic' water-involved side reactions on the metal surface, as demonstrated (insert table) in Figures 3c–d. Following 20 cycles, compared with the original pure Zn electrode (Figure S22), the Zn surface was corroded and exhibited dendrites because of the parasitic side reactions of 0.5 M-$Zn(OTf)_2$-H_2O electrolyte with the Zn interface. After 200 cycles, the corrosion of Zn metal became highly significant, with some areas exhibiting depletion, and large dendrites. In comparison, with organic DMMP and hybrid DMMP-H_2O electrolyte, the cycled Zn electrode for 20 and 200 cycles did not exhibit apparent depletion or dendrites, Figures 3e–f. MD simulation findings for DMMP-H_2O electrolyte (Figure S23) confirmed that introduction of water into the solvent maintained a DMMP dominated solvation structure, as evidenced by the radial distribution of electrolyte component around Zn^{2+} ion.

It is concluded therefore that the hybrid DMMP-H_2O electrolyte utilizes DMMP solvent in phosphating conversion and boosts Zn electrode stability. Additionally, the water increases wettability of the electrolyte to the metal anode, and promotes a uniform ion transportation (Figure S24). The aqueous 0.5 M-$Zn(OTf)_2$-H_2O electrolyte causes highly significant corrosion and dendrite growth on the Zn electrode surface, because of formation of hydrate by products and competitive H_2 evolution, Figure 3g. In addition to benefiting from the phosphating passivation of the high D solvent, DMMP based organic or hybrid electrolyte (Figure 3h–i), suppresses dendrite formation on the Zn surface and promotes highly reversible zinc ion diffusion.

Monolithic Phosphate SEI on Zn Anode

The SEI in DMMP electrolyte exhibits a high ratio of phosphorous from DMMP, which can be identified as zinc phosphates (Figure S11). Similar SEI was evidenced with DMMP-H_2O hybrid electrolyte, as confirmed via cryo-scanning transmission electron microscopy (cryo-STEM) and XPS findings, Figure 4. The passivated interphase formed under the hybrid electrolyte on the Zn metal anode exhibits a similar, dense cross-section morphology (Figure S25) with that formed in DMMP electrolyte (Figure S9). To obtain a controlled thickness of SEI to observe lattice structure under high-energy electrons in cryo-STEM, the

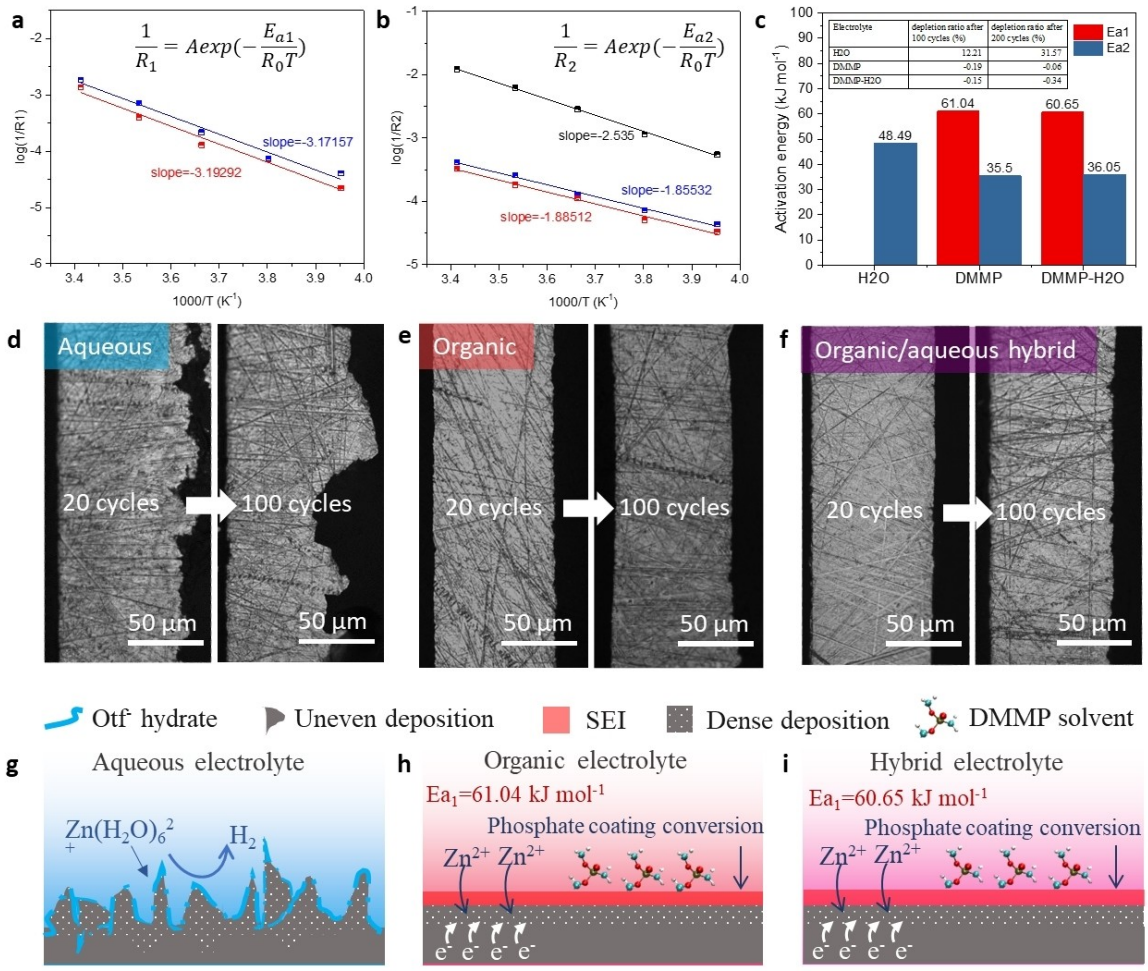

Figure 3. Physical property of interface formed under aqueous, organic and hybrid, electrolyte. (a, b) Arrhenius plots for Zn | Zn symmetric cells at temperature, where blue-colour, red and black lines represents, respectively, battery with 0.5 M-Zn(OTf)$_2$-DMMP, 0.5 M-Zn(OTf)$_2$-DMMP-H$_2$O hybrid and aqueous 0.5 M-Zn(OTf)$_2$-H$_2$O electrolyte. Zn | Zn cells using different electrolyte were pre-cycled for 20 cycles at 1 mA cm^{-2} with an areal capacity of 1 mAh cm^{-2}. Activation energy E_{a1} for transport of Zn^{2+} in interphase on Zn surface was computed from R_1 (in equivalent circuit), which arises from impedance of interfacial film in high-middle frequency. Activation energy E_{a2}, for desolvation barrier for Zn^{2+} in electrolyte, from R_2, which arises from charge-transfer. (c) Comparison of activation energy E_{a1} and E_{a2} with different electrolyte, with insert showing depletion ratio of Zn electrodes was computed from symmetric battery for 100 and 200 cycles. Cross-section view of Zn electrode following different cycles in (d) aqueous 0.5 M-Zn(OTf)$_2$-H$_2$O, (e) organic 0.5 M-Zn(OTf)$_2$-DMMP, and (f) hybrid 0.5 M-Zn(OTf)$_2$-DMMP-H$_2$O, electrolyte. Illustration of interfacial reactions on Zn with (g) aqueous 0.5 M-Zn(OTf)$_2$-H$_2$O, (h) organic 0.5 M-Zn(OTf)$_2$-DMMP and (i) 0.5 M-Zn(OTf)$_2$-DMMP-H$_2$O, electrolyte.

FIB was applied to cut the sample into a lamella, Figure S26. The prepared thin lamella sample, Figure 4a, exhibits a clear boundary between SEI and zinc substrate, with the protective carbon-layer that was coated during sample preparation seen on the top of robust SEI.

The enlarged area of SEI in Figure 4b has a homogeneous monolithic structure, with thickness *ca.* 300 nm. The Energy Dispersive Spectroscopy (EDS) and mapping of Figure 4c (and Figure S27) evidence that the SEI contains only Zn, P and O, underscoring the uniform composition of this interphase. This finding is in contrast with reported mosaic- or multilayer-type SEI derived from decompositions of both the solvent and salt anion.

Seen under STEM high-resolution mode, the lattice structure of the interphase is evident, Figure 4d (and Figure S28). This confirms that Zn, P and O formed both crystalized and amorphous phases. As shown in the marked crystalized area i, the lattice fringes are identified as the (020) and (220) planes from $Zn_3(PO_4)_2$. In addition, crystalized phase zinc metaphosphate (ZnP_2O_6) was identified in the marked area ii, and the amorphous area is possibly mixed compounds of the two zinc phosphates. This combination of homogeneous crystalized and amorphous phases has good adhesion to the Zn metal substrate, as has been reported for phosphate bath coating in steel.[26] With the full XPS results before etching shown in Figure S29, the etching of the P2p and O1s spectra in Figures 4e–f confirm the homogeneous and monolithic form of SEI composition, and with increase in etching time, the atomic ratio of the zinc phosphates reduced accordingly.

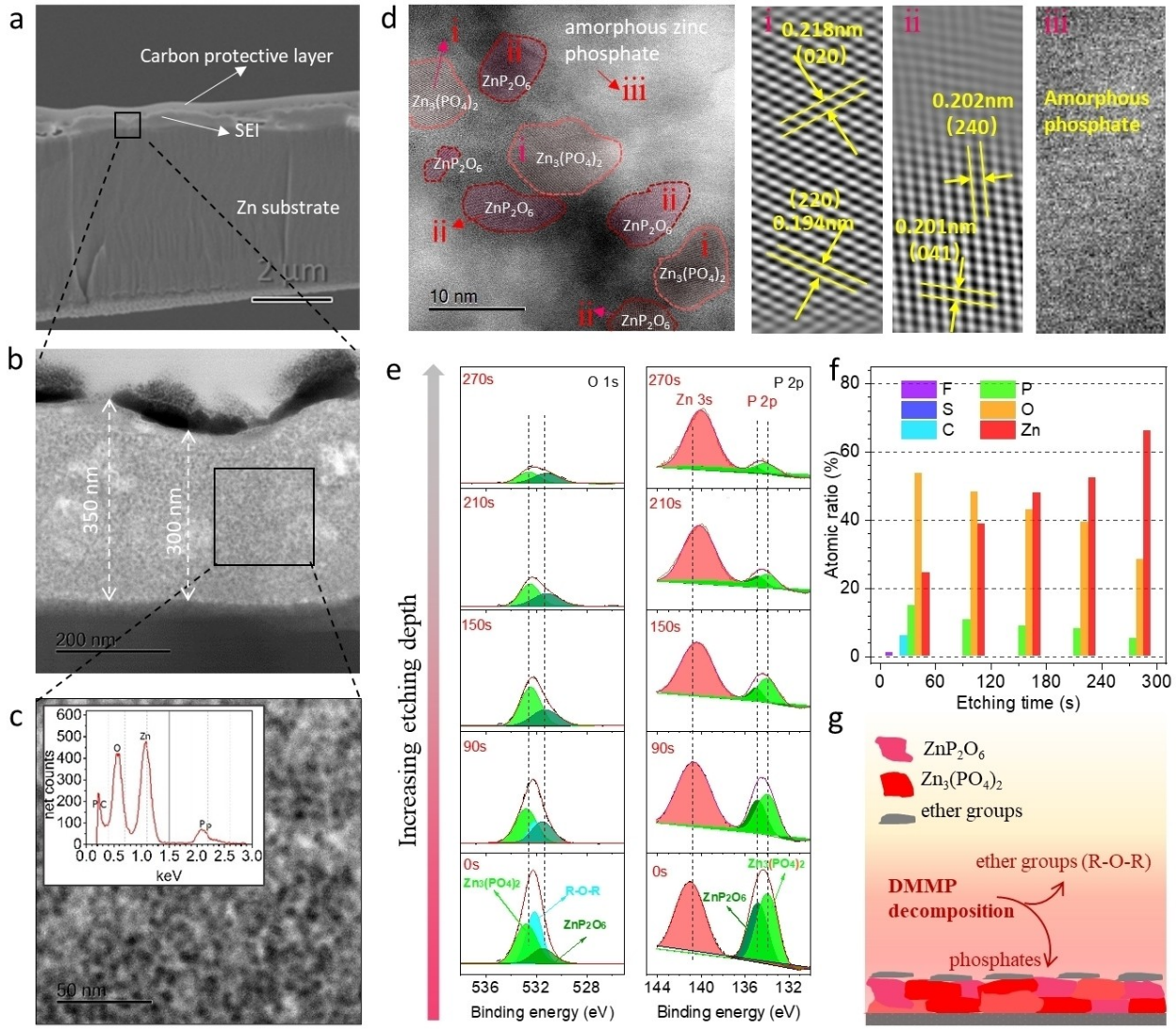

Figure 4. Identification of SEI compositions from hybrid 0.5 M-$Zn(OTf)_2$-DMMP-H_2O electrolyte. (a) SEM-FIB image of SEI formed on Zn substrate prepared in lamella under protection of C-layer. (b, c) Cryo-TEM images of SEI area in the lamella sample. (d) HR-STEM image of SEI area from lamella sample with corresponding lattices from representative three areas (i–iii). (e) XPS spectra for P2p and O1s elements from cycled Zn anode surface with accumulation of etching time. (f) Computed atomic ratio for elements derived from XPS data with increase of etching time. (g) Schematic for possible interfacial reaction pathway under hybrid 0.5 M-$Zn(OTf)_2$-DMMP-H_2O electrolyte.

Based on the monolithic composition of the SEI formed in DMMP-H_2O electrolyte, it is hypothesized that DMMP solvent undergoes a simple phosphating conversion reaction, as is illustrated in Figure 4g. During decomposition of DMMP, the zinc phosphates are coated on the Zn electrode, whilst ether compounds[27] are released into the electrolyte. The phosphating SEI readily transports Zn^{2+} because of high ionic conductivity of zinc phosphates. The multicomponent nature of the monolithic SEI of crystalized and amorphous phosphates provides channels such as vacancies, interstitials, and grain boundaries for rapid Zn^{2+} transport.

Electrochemical Performance in Half and Full Cells

The protective impact of the phosphating SEI in hybrid DMMP-H_2O electrolyte was determined through a comparison of corrosion (Figure 5a and Figure S30) of the electrolytes on Zn metal and from electrochemical performance in Figures 5b–d. DMMP-H_2O electrolyte exhibited a greater corrosion potential of −939.808 mV compared with −964.303 mV in 0.5 M-$Zn(OTf)_2$-H_2O electrolyte, evidencing reduced tendency to Zn corrosion. The corrosion potential for DMMP-H_2O to Zn metal is close to that in DMMP electrolyte of −939.2 mV, demonstrating the protecting ability of the interphase under water. Additionally,

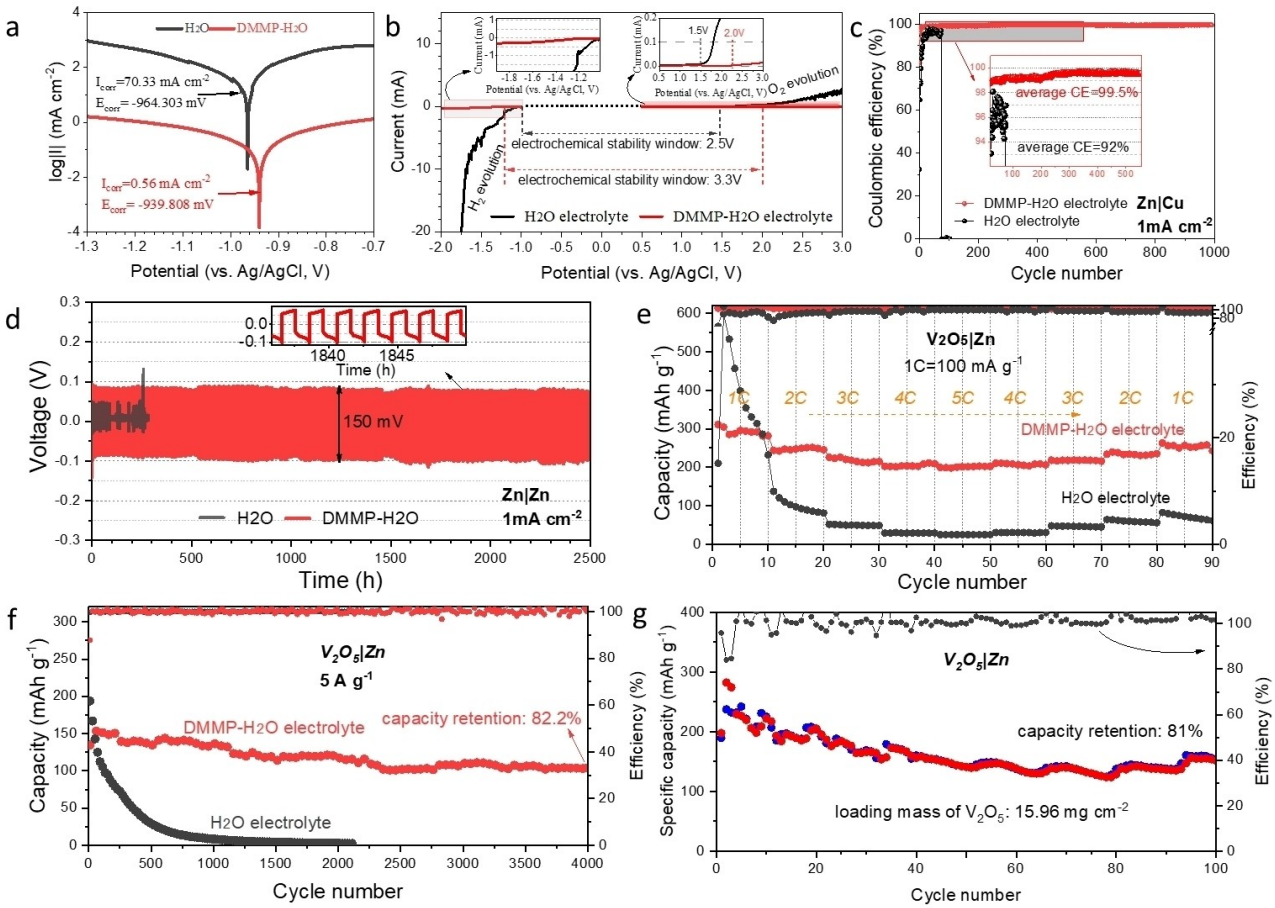

Figure 5. Electrochemical performance for hybrid 0.5 M-Zn(OTf)$_2$-DMMP-H$_2$O electrolyte. (a) Linear polarization curve on bare Zn showing corrosion under aqueous 0.5 M-Zn(OTf)$_2$-H$_2$O and hybrid 0.5 M-Zn(OTf)$_2$-DMMP-H$_2$O, electrolyte. (b) Electrolyte stability window for baseline aqueous electrolyte and designed hybrid electrolyte with linear sweep voltammetry (LSV) scanning, where HER and OER properties were analysed using Ti as working and counter electrode against an Ag/AgCl reference electrode. (c) CE for baseline aqueous and designed hybrid, electrolyte at current density 1 mA cm^{-2} in Zn|Cu battery. (d) Long-term cycling performance for Zn|Zn symmetric battery under designed and baseline electrolyte. (e) Rate and (f) cycling performance for V_2O_5|Zn full cells with H$_2$O and DMMP-H$_2$O electrolyte. (g) Cycling curve for V_2O_5|Zn full pouch cell under current density 100 mA g^{-1} with designed DMMP-H$_2$O electrolyte.

DMMP-H$_2$O electrolyte exhibits good interfacial compatibility and increases the electrochemical stability window for aqueous electrolyte from 2.5 to 3.3 V, as seen in Figure 5b. A Zn|Cu cell using DMMP-H$_2$O electrolyte exhibited a high CE of 99.5 % for 1000 cycles with a low polarization of 0.85 V, Figure 5c (and Figure S31). In comparison, a cell with 0.5 M-Zn(OTf)$_2$-H$_2$O electrolyte exhibited reversible cycling for <80 cycles and a low average CE of 92 %. The symmetric cell with the as-designed hybrid electrolyte exhibited a long cycling of 2000 cycles and low overpotential of 150 mV, Figure 5d. This performance of the half cell evidences the protecting ability of the DMMP solvent passivated interphase, and importance for highly reversible Zn metal.

To demonstrate practicality of the DMMP-based electrolyte, full cell performances were determined via Prussian blue, KV_3O_8 and V_2O_5 as cathode. For pure, organic DMMP electrolyte, the choice of cathode is important because many materials require water to boost reaction. V_2O_5 as cathode cannot exhibit high capacity with pure, organic DMMP electrolyte, however (classic) Prussian blue exhibited a reversible capacity of >40 mA g^{-1} for >200 cycle (Figure S32). The addition of water in DMMP to synthesize DMMP-H$_2$O hybrid electrolyte improves ionic conductivity from 3 to 4.9 mS cm^{-1} and boosts reaction of Zn^{2+} ions with vanadium oxide cathode. DMMP-H$_2$O electrolyte works with KV_3O_8 cathode material, to maintain a highly reversible rate capacity (Figure S33 and S34). DMMP-H$_2$O electrolyte enables a V_2O_5 cathode to exhibit stable rate, Figure 5e, and cycling performance under both low and high current densities, Figure 5f (and Figure S35). As is shown in Figure 5e, superior rate capability under low current rate from 100 to 500 mA g^{-1} is exhibited in the as-designed hybrid electrolyte, with a specific capacity of 204.3 mAh g^{-1} at 500 mA g^{-1}. Under 5 A g^{-1}, the V_2O_5|Zn full battery with DMMP-H$_2$O electrolyte exhibits a high capacity retention of

82.2 % following 4000 charge/discharge cycles, significantly higher than that with the H_2O electrolyte, which exhibited rapid capacity decay following 500 cycles. The 'slight' capacity loss under DMMP-H_2O electrolyte is likely because of dissolution of V_2O_5 in water. Significantly, the pouch cell $V_2O_5|Zn$ with DMMP-H_2O worked for 100 cycles and with an energy density of 51.52 $Wh\,kg^{-1}$, and high V_2O_5 loading mass of 15.96 $mg\,cm^{-2}$, Figure 5g.

Conclusion

We introduce a high dipole moment solvent DMMP with the predominated reduction property as a strong SEI resource for zinc metal anode in both the organic (DMMP) and hybrid (molar ratio of $DMMP:H_2O=3:2$) electrolytes via the fast conversion of DMMP into homogeneous and dense phosphate compounds. The in situ occurred phosphating conversion coating on zinc anode from this DMMP solvent forms a monolithic SEI, consisting of only inorganic phosphate phases ($Zn_3(PO_4)_2$ and ZnP_2O_6). This SEI is different from the previous reports on Zn anode that normally have over two different species enriched in certain area, and instead, it exhibits a uniform and robust structure that permits Zn^{2+} diffusion through phosphates and the boundary between the phosphates. As a result, this SEI inhibits dendrites growth and reduce zinc corrosion. The protecting impact of the SEI from phosphating reaction on the Zn metal anode is evidenced by the finding that Zn|Zn cells with DMMP based electrolytes exhibited long-term cycling stability of 4700 h and a high Zn^{2+} plating/stripping reversibility in Zn|Cu cells with CE = 99.89 % at 0.5 $mA\,cm^{-2}$. Additionally, a full $V_2O_5|Zn$ cell with the DMMP-H_2O hybrid electrolyte exhibited a high capacity retention of 82.2 % after 4000 cycles under 5 $A\,g^{-1}$. These results showcase advantages of a monolithic interphase, and reveal an effective strategy to construct monolithic interphase by utilizing phosphate solvent with high dipole moment to realize phosphating dominated reactions. Our findings and understanding of this monolithic interphase in associated electrolytes will be of benefit in practical SEI design for highly reversible and stable metal anode in metal ion batteries.

Author Contributions

S. L. Liu, J. F. Mao, and Z. P. Guo conceived the idea. S. L. Liu conducted experiments and prepared the manuscript. J. F. Mao and Z. P. Guo supervised the project and revised the manuscript. Other authors contributed to data collection, analyses and final manuscript.

Acknowledgements

This work was financially supported by the Australian Research Council Discovery Projects (DP200101862, FL210100050) and Australian Synchrotron infrared Micro-spectroscopy beamline (M16823, M17455 and M18527). The authors gratefully acknowledge technical support from the Electron Microscopy Centre the University of Wollongong. Open Access publishing facilitated by The University of Adelaide, as part of the Wiley - The University of Adelaide agreement via the Council of Australian University Librarians.

Conflict of Interest

The authors declare that they have no competing interests.

Data Availability Statement

The data that support the findings of this study are available from the corresponding author upon reasonable request.

Keywords: Fire Retardant · Hybrid Electrolyte · Phosphate Solvent · Solid Electrolyte Interphase · Zinc Ion Batteries

[1] a) Q. Zhang, J. Luan, Y. Tang, X. Ji, H. Wang, *Angew. Chem. Int. Ed.* **2020**, *59*, 13180–13191; *Angew. Chem.* **2020**, *132*, 13280–13291; b) Y. Wang, Z. Wang, F. Yang, S. Liu, S. Zhang, J. Mao, Z. Guo, *Small* **2022**, *18*, 2107033; c) S. Liu, R. Zhang, J. Mao, Y. Zhao, Q. Cai, Z. Guo, *Sci. Adv.* **2022**, *8*, eabn5097.

[2] a) N. Zhang, X. Chen, M. Yu, Z. Niu, F. Cheng, J. Chen, *Chem. Soc. Rev.* **2020**, *49*, 4203–4219; b) C. Xu, Y. Zhang, N. Zhang, X. Liu, J. Yi, X. Liu, X. Lu, Q. Ru, H. Lu, X. Peng, X. S. Zhao, J. Ma, *Chem. Asian J.* **2020**, *15*, 3696–3708; c) Z. Zhao, R. Wang, C. Peng, W. Chen, T. Wu, B. Hu, W. Weng, Y. Yao, J. Zeng, Z. Chen, P. Liu, Y. Liu, G. Li, J. Guo, H. Lu, Z. Guo, *Nat. Commun.* **2021**, *12*, 6606.

[3] L. Cao, D. Li, F. A. Soto, V. Ponce, B. Zhang, L. Ma, T. Deng, J. M. Seminario, E. Hu, X.-Q. Yang, P. B. Balbuena, C. Wang, *Angew. Chem. Int. Ed.* **2021**, *60*, 18845–18851; *Angew. Chem.* **2021**, *133*, 18993–18999.

[4] J. Yang, B. Yin, Y. Sun, H. Pan, W. Sun, B. Jia, S. Zhang, T. Ma, *Nano-Micro Lett.* **2022**, *14*, 42.

[5] a) N. V. Phuong, K. Lee, D. Chang, M. Kim, S. Lee, S. Moon, *Met. Mater. Int.* **2013**, *19*, 273–281; b) K. Ogle, M. Wolpers, *ASM Handbook* **2003**, *13*, 712–719.

[6] B. Liu, X. Zhang, G.-y. Xiao, Y.-p. Lu, *Mater. Sci. Eng. C* **2015**, *47*, 97–104.

[7] X. Zeng, K. Xie, S. Liu, S. Zhang, J. Hao, J. Liu, W. K. Pang, J. Liu, P. Rao, Q. Wang, J. Mao, Z. Guo, *Energy Environ. Sci.* **2021**, *14*, 5947–5957.

[8] a) L. Cao, D. Li, E. Hu, J. Xu, T. Deng, L. Ma, Y. Wang, X.-Q. Yang, C. Wang, *J. Am. Chem. Soc.* **2020**, *142*, 21404–21409; b) J. Hao, L. Yuan, C. Ye, D. Chao, K. Davey, Z. Guo, S. Qiao, *Angew. Chem. Int. Ed.* **2021**, *60*, 7366–7375; *Angew. Chem.* **2021**, *133*, 7442–7451; c) D. Wang, Q. Li, Y. Zhao, H. Hong, H. Li, Z. Huang, G. Liang, Q. Yang, C. Zhi, *Adv. Energy Mater.* **2022**, *12*, 2102707.

[9] L. Cao, D. Li, T. Deng, Q. Li, C. Wang, *Angew. Chem. Int. Ed.* **2020**, *59*, 19292–19296; *Angew. Chem.* **2020**, *132*, 19454–19458.

[10] a) A. Naveed, H. Yang, J. Yang, Y. Nuli, J. Wang, *Angew. Chem. Int. Ed.* **2019**, *58*, 2760–2764; *Angew. Chem.* **2019**, *131*, 2786–2790; b) A. Naveed, H. Yang, Y. Shao, J. Yang, N. Yanna, J. Liu, S. Shi, L. Zhang, A. Ye, B. He, J. Wang, *Adv. Mater.* **2019**, *31*, 1900668.

[11] D. Li, L. Cao, T. Deng, S. Liu, C. Wang, *Angew. Chem. Int. Ed.* **2021**, *60*, 13035–13041; *Angew. Chem.* **2021**, *133*, 13145–13151.
[12] Y. Chu, S. Zhang, S. Wu, Z. Hu, G. Cui, J. Luo, *Energy Environ. Sci.* **2021**, *14*, 3609–3620.
[13] S. Liu, J. Mao, W. K. Pang, J. Vongsvivut, X. Zeng, L. Thomsen, Y. Wang, J. Liu, D. Li, Z. Guo, *Adv. Funct. Mater.* **2021**, *31*, 2104281.
[14] X. Cao, X. Ren, L. Zou, M. H. Engelhard, W. Huang, H. Wang, B. E. Matthews, H. Lee, C. Niu, B. W. Arey, *Nat. Energy* **2019**, *4*, 796–805.
[15] a) M. Tesemma, F.-M. Wang, A. M. Haregewoin, N. L. Hamidah, P. Muhammad Hendra, S. D. Lin, C.-S. Chern, Q.-T. Pham, C.-H. Su, *ACS Sustainable Chem. Eng.* **2019**, *7*, 6640–6653; b) M. Mutoh, S. Abe, T. Kusaka, M. Nakamura, Y. Yoshida, J. Iida, H. Tachikawa, *Atoms* **2015**, *4*, 4.
[16] a) H. Xiang, H. Xu, Z. Wang, C. Chen, *J. Power Sources* **2007**, *173*, 562–564; b) Z. Zeng, V. Murugesan, K. S. Han, X. Jiang, Y. Cao, L. Xiao, X. Ai, H. Yang, J.-G. Zhang, M. L. Sushko, *Nat. Energy* **2018**, *3*, 674; c) J. Xu, X. Ji, J. Zhang, C. Yang, P. Wang, S. Liu, K. Ludwig, F. Chen, P. Kofinas, C. Wang, *Nat. Energy* **2022**, *7*, 186–193.
[17] X. Song, H. He, M. H. Aboonasr Shiraz, H. Zhu, A. Khosrozadeh, J. Liu, *Chem. Commun.* **2021**, *57*, 1246–1249.
[18] W. Kaveevivitchai, A. Manthiram, *J. Mater. Chem. A* **2016**, *4*, 18737–18741.
[19] W. Kao-ian, M. T. Nguyen, T. Yonezawa, R. Pornprasertsuk, J. Qin, S. Siwamogsatham, S. Kheawhom, *Mater. Today Energy* **2021**, *21*, 100738.
[20] N. Wang, X. Dong, B. Wang, Z. Guo, Z. Wang, R. Wang, X. Qiu, Y. Wang, *Angew. Chem. Int. Ed.* **2020**, *59*, 14577–14583; *Angew. Chem.* **2020**, *132*, 14685–14691.
[21] D. Han, C. Cui, K. Zhang, Z. Wang, J. Gao, Y. Guo, Z. Zhang, S. Wu, L. Yin, Z. Weng, F. Kang, Q.-H. Yang, *Nat. Sustainability* **2022**, *5*, 205–213.
[22] O. Borodin, X. Ren, J. Vatamanu, A. von Wald Cresce, J. Knap, K. Xu, *Acc. Chem. Res.* **2017**, *50*, 2886–2894.
[23] J. M. Bowen, C. R. Powers, A. Ratcliffe, M. G. Rockley, A. W. Hounslow, *Environ. Sci. Technol.* **1988**, *22*, 1178–1181.
[24] a) S. A. Suthanthiraraj, R. Kumar, B. J. Paul, *Spectrochim. Acta Part A* **2009**, *71*, 2012–2015; b) F. Mortimer, *Spectrochim. Acta* **1957**, *9*, 270–281.
[25] a) Y. Kim, Y. Park, M. Kim, J. Lee, K. J. Kim, J. W. Choi, *Nat. Commun.* **2022**, *13*, 2371; b) M. Yan, P. He, Y. Chen, S. Wang, Q. Wei, K. Zhao, X. Xu, Q. An, Y. Shuang, Y. Shao, K. T. Mueller, L. Mai, J. Liu, J. Yang, *Adv. Mater.* **2018**, *30*, 1703725; c) F. Wang, W. Sun, Z. Shadike, E. Hu, X. Ji, T. Gao, X. Q. Yang, K. Xu, C. Wang, *Angew. Chem. Int. Ed.* **2018**, *57*, 11978–11981; *Angew. Chem.* **2018**, *130*, 12154–12157.
[26] C. Jiang, Z. Gao, H. Pan, X. Cheng, *Electrochem. Commun.* **2020**, *114*, 106676.
[27] M. B. Mitchell, V. N. Sheinker, W. W. Cox, E. N. Gatimu, A. B. Tesfamichael, *J. Phys. Chem. B* **2004**, *108*, 1634–1645.

Manuscript received: October 23, 2022
Accepted manuscript online: November 29, 2022
Version of record online: December 16, 2022